Integrated Transcriptome, Proteome, Acetylome, and Metabolome Profiling of Mouse Liver During Normal Aging

Jiang-Feng Liu
Peking Union Medical College
Song-Feng Wu
Beijing Proteome Research Center
Cong Liu
Shanghai Institute of Organic Chemistry
Hou-Zao Chen
Peking Union Medical College
Juntao Yang (yangjt@pumc.edu.cn)
CAMS PUMC: Chinese Academy of Medical Sciences and Peking Union Medical College
https://orcid.org/0000-0003-1180-391X

Research article

Keywords: multi-omics, mouse, liver, normal aging, metabolic process

Posted Date: November 13th, 2020

DOI: https://doi.org/10.21203/rs.3.rs-104808/v1

Abstract

Background

Aging is a complex biological process accompanied by a time-dependent functional decline that affects most living organisms. We aimed to obtain an integrated aging-associated profile of the mouse liver using a multi-omics approach.

Results

We performed a combined transcriptome, proteome, acetylome, and metabolome analysis of liver tissues from young and old mice under physiological conditions. Old mice were frequently obese with a fatty liver, and the observed profile changes in different omics were generally moderate. Specifically, transcriptome, proteome, and acetylome analyses revealed different patterns in old and young mice, but metabolome analysis did not. Functional enrichment analysis showed that metabolic pathways were broadly altered during normal aging. Notably, the genes, proteins, and metabolites involved in pyrimidine and glutathione metabolisms were significantly affected in all these four omics. Moreover, we observed increased arachidonic acid metabolism and decreased complement and coagulation cascades in old mice, suggesting an alteration in the immune function during normal aging.

Conclusions

We conducted a multi-omics investigation of normal liver aging in mice and generated comprehensive datasets for aging research. Further analysis revealed that impairment of pyrimidine and glutathione metabolisms and immune function may be critical for hepatic aging and may provide targets for aging interventions.

Background

Aging is a complex biological process accompanied by a time-dependent functional decline that affects most living organisms [1]. Aging and aging-associated diseases have brought great suffering and economic burden to individuals and society [2]. Aging-associated alterations include genomic instability, epigenetic alterations, loss of proteostasis, and metabolic manipulation [1, 3]. Several interventions, including rapamycin, senolytics, NAD precursors, sirtuin-activating compounds, metformin, exercise, and calorie restriction, can potentially increase the health span and/or lifespan [4]. However, pivotal methods for interventions in aging are still deficient as our global view of normal aging is rather incomplete.

Omics analyses offer the advantage of obtaining an overall profile of biological processes. Transcriptome [5], proteome [6], metabolome [7], single-cell transcriptome [8], and many other omics analyses have been utilized alone or in combination to study aging and present an increasingly detailed landscape of the aging process in different species. The liver is the biggest metabolic organ in mammals. Liver aging deserves adequate research, as metabolism and epigenetics are intricately linked and work

together to influence aging [3]. Although the physiological aging of the liver shows relatively modest changes [9, 10], omics studies have discovered some significant molecular alterations. During aging, DNA methylation in the liver is largely remodeled, can be accelerated by obesity, and may affect downstream gene expression [11, 12]. In the aged mouse liver, inflammation is common [13, 14], and disruption of metabolic homeostasis and circadian metabolism are observed [15, 16]. As aging is a highly complex process spanning gene expression to metabolism, we expect that a comprehensive multi-omics analysis would improve our understanding of liver aging.

In this study, we performed a multi-omics analysis of the transcriptome, proteome, acetylome, and metabolome of livers from 2-month-old and 18-month-old mice under normal physiological conditions. We found that old mice frequently had obesity and a fatty liver. Transcriptome, proteome, and acetylome profiles distinguished young and old livers, but metabolome profiles did not. Further analysis revealed that dysregulation of pyrimidine and glutathione metabolisms and immune function might be critical for hepatic aging, which may provide targets for aging interventions. In addition, our results provide comprehensive multi-omics datasets for future aging research.

Results

Liver fat deposition in mice increases during aging

Fourteen 2-month-old young mice (1–14) and ten 18-month-old aged mice (1–10) were euthanized, and their livers removed for multi-omics analyses. Transcriptome and metabolome analyses were performed with individual liver samples, and proteomics and acetylomics analyses were performed on pooled ones (Fig. 1A). Old mice weighed 32.72 ± 1.937 g and were significantly heavier than young mice (25.79 ± 0.482 g; Fig. 1B). The liver index (liver weight/body weight) of old mice was 5.055 ± 0.2444%, slightly higher than that of young mice (4.459 ± 0.1218%; Fig. 1C). H & E and Masson staining showed no obvious differences between the livers of old and young mice (Fig. 1D). Oil red O staining showed clear fat accumulation in old livers but not in young ones (Fig. 1D), consistent with a previous report [17]. In summary, the old mice seemed susceptible to fatty liver.

Transcriptome profiles distinguish old and young mice livers

We carried out high-throughput RNA-Seq on old and young mice livers to assess transcriptional changes during aging (brief quality information in Table S1). Over 50% FPKM > 1 in at least one group enabled the identification of 13,275 transcripts. Replicate correlation calculation revealed that the transcriptomic expression mode between samples was highly similar (Pearson correlation coefficient above 0.92, Fig. S1A). Hierarchical clustering analysis (unsupervised Euclidean distance) clearly separated livers of the old and young mice (Fig. 2A), and the same classification was supported by principal component analysis (PCA; Fig. 2B). The aged liver transcriptomes were more individually variable than the young ones, as the Euclidean distance values between old mice were higher (Fig. 2A). FC and adjusted p-value

were calculated for differential expression analysis using the edgeR R package. A total of 1,439 transcripts were assigned as differentially expressed (810 up-regulated and 629 down-regulated in old mice), as shown in the volcano plot (Fig. 2C). We considered transcripts with over 50% FPKM > 1 in young mice, but less than 50% FPKM > 1 in old mice as young-unique, and transcripts with the contrary feature were considered old-unique. Up-regulated transcripts in old mice contained 169 old-unique ones, and down-regulated transcripts contained 130 young-unique ones (Fig. 2D). To predict localization, total, up-, and down-regulated transcripts were submitted to Ingenuity Pathway Analysis (IPA). Compared to the total transcriptome, up-regulated transcripts contained a reduced proportion of nuclear genes and increased plasma membrane genes, and down-regulated transcripts contained a reduced proportion of cytoplasm genes (Fig. S1B). For functional enrichment analysis, up- and down-regulated transcripts in old mice were submitted to KOBAS, a web server, to perform KEGG analysis. Notably, differentially expressed transcripts during aging were enriched in various metabolic pathways, some of which both contained up- and down-regulated transcripts (Fig. 2E, 2F). Cytochrome P450, glutathione S-transferase, and UDP glucuronosyltransferase 2 family genes were enriched in both up- and down-regulated pathways (Table S2). Several lysosome-associated and oncogenic genes, such as Prkca (PKCα) and Wnt5a, were up-regulated, whereas multiple histones and innate immune system-associated proteins decreased during aging (Table S2).

Proteomic profiling of young and old mouse livers

Proteome data were obtained using LC-MS/MS. A total of 541,511 spectra were submitted to MaxQuant, and 77,726 (14.35%) were matched to 70,092 peptides (of which 40,796 were unique). This study identified 5,831 proteins and quantified 4,712 (Fig. S2A). For quality control, we assessed peptide length (Fig. S2B), spectra count per peptide (Fig. S2C), Andromeda score distribution (Fig. S2D), and Pearson correlation coefficient between samples (Fig. S2E). After ID conversion (Ensemble IDs of transcripts and SwissProt IDs of proteins were both converted to Symbol IDs), 4,316 proteins were matched to mRNAs, the expression of which revealed a low positive expression correlation (Spearman correlation coefficient = 0.366829). Both hierarchical clustering analysis (Fig. 3A) and PCA (Fig. 3B) of the quantified proteins showed that the hepatic proteome of young mice clearly differed from that of old mice. We performed Significance A analysis using Perseus (both sides, Benjamini-Hochberg FDR < 0.05) to define differentially expressed proteins and found 114 increased and 81 decreased proteins in old livers. Similar to the transcriptome analysis, we assessed cellular localization of the total, up-, and down-regulated proteins. Generally, the proportion of cytoplasm genes in the proteome was higher than that in the transcriptome and differentially expressed proteins contained a greater proportion of extracellular proteins than the total proteome (Fig. 3C). KEGG enrichment analysis showed that differentially expressed proteins were especially enriched in metabolic pathways (Fig. 3D, 3E). At the protein level, cytochrome P450 and glutathione S-transferase family proteins were also found in both up- and down-regulated pathways. The levels of cytochrome c oxidase subunits, prostamide/prostaglandin F synthase, and leukotriene-B(4) omega-hydroxylase 2 tended to increase, and those of glutaminase tended to decrease in the mouse liver during aging (Table S3).

Extensive acetylation of histones and metabolic pathway proteins

Acetylome data were also obtained using LC-MS/MS. A total of 146,519 spectra were submitted to MaxQuant, and 18,601 (12.7%) were matched to 13,808 peptides (1,690 proteins). A total of 13,606 peptides (6,626 of which unique) in 1,669 proteins were recorded as acetylated, and 5,640 unique acetylated sites were identified (Fig. S3A). For quality control, we assessed peptide length (Fig. S3B), spectral count per acetyl peptide (Fig. S3C), mass error (Fig. S3D), and Andromeda score distribution (Fig. S3E). Each acetylated peptide could contain at most four acetylation sites, but most acetylated peptides contained only one (Fig. S3F). The localization probabilities of acetylation sites ranged from 0 to 1, and every quantile was grouped into one class. Class I sites (localization probability > 0.75) occupied 99.4% of all the acetylated ones (Fig. S3G), and 4,818 of them (1,367 proteins) were quantifiable. Pearson correlation coefficient showed a high similarity between samples (Fig. S3H). Hierarchical clustering analysis (Fig. 4A) and PCA (Fig. 4B) of the quantifiable

Class I acetylation sites revealed that acetylome profiles distinguished livers of old and young mice. Motif analysis showed that glutamate or aspartate was frequently adjacent to an acetylated lysine (Fig. 4C). Acetylated proteins were mostly located in the cytoplasm. Compared to all acetylated proteins, the down-regulated ones contained no plasma membrane proteins, and up-regulated ones contained a smaller proportion of nuclear proteins (Fig. 4D). The proteome and acetylome shared 1,262 proteins (Fig. 4E), which were enriched in multiple metabolic pathways and ribosomal proteins (Fig. 4F). Except for metabolic pathways, non-acetylated proteins were mainly enriched in spliceosome, endocytosis, protein processing in the endoplasmic reticulum (ER), and lysosome, which are associated with intracellular macromolecular homeostasis (Fig. 4G). Histones were the major proteins with altered profiles identified only in the acetylome (Fig. 4H). However, histone profiles in the transcriptome, proteome, and acetylome analysis showed no consistent alteration (Table S4). The Spearman correlation coefficient was only 0.38168 between proteome and acetylome profiles. We thus performed Significance A analysis for acetylome alone to define differentially expressed acetylated sites and proteins, finding 60 acetylation sites in 39 proteins increased, and 53 sites in 38 proteins decreased during aging. KEGG analysis showed that proteins containing differentially expressed acetylation sites were predominantly enriched in metabolic pathways and protein processing (Fig. S4A, S4B). Proteins in the enriched metabolic pathways are associated with fatty acid, amino acid, and nucleic acid metabolism, but contained only one cytochrome (cytochrome P450 4A14) whose family members broadly changed in the transcriptome and proteome profiles (Table S5).

Transcriptome, proteome, acetylome, and metabolome profiles show dysregulated pyrimidine and glutathione metabolisms during hepatic aging

To identify the key alteration in the mouse liver during aging, we obtained the intersection of enriched pathways (corrected p-value < 0.05) differentially regulated in the transcriptome, proteome, and acetylome. Up-regulated transcripts and up-regulated proteins were both enriched in 16 KEGG pathways, 5 of which contained differentially expressed acetylation sites (Fig. 5A). Down-regulated transcripts and proteins shared 17 KEGG pathways, 7 of which contained differentially regulated acetylation sites (Fig. 5B). Considering that metabolites reflect the results of complex biological processes, we performed metabolome analysis of the liver samples using LC-MS/MS to further narrow the functional alterations during hepatic aging.

In this study, 242 and 399 metabolites were identified in negative- and positive-ion modes, respectively. Pearson correlation coefficients between the four samples for quality control (QC samples) were nearly 1.00, and those between testing samples were all greater or equal than 0.80 (Fig. S5A, S5D), suggesting high-quality metabolome data. PCA showed that QC samples were condensed, but neither negative- or positive-ion mode could distinguish young and old livers (Fig. 6A, 6B). Although OPLS-DA analysis barely separated the two groups (Fig. S5B, S5E), permutation test results revealed that the metabolite profiles of young and old mouse livers were similar (Fig. S5C, S5F). More metabolites with reduced than increased levels were identified by negative-ion mode and metabolites identified in positive-ion mode were distributed more symmetrically (Fig. 6C, 6D). We selected metabolites based on MS2 score and FC, 43 of which were up-regulated and 63 down-regulated (Table S6). MetaboAnalyst pathway analysis suggested that up-regulated metabolites were significantly ($p < 0.05$) associated with riboflavin, starch, sucrose, fructose, and mannose metabolisms (Fig. 6E), whereas down-regulated metabolites were significantly associated with pyrimidine, glycerophospholipid, and glutathione metabolisms (Fig. 6F). Taking all the four omics results into consideration, dysregulated pyrimidine and glutathione metabolisms are especially notable during aging.

Discussion

In this study, we performed the first combined transcriptome, proteome, acetylome, and metabolome analyses of young and old mouse livers under physiological conditions. Transcriptome, proteome, and acetylome profiles revealed different expression patterns in old and young mice, in contrast to metabolomic profiles. Although many metabolic alterations were observed in all four omics, pyrimidine and glutathione metabolisms were clearly dysregulated during hepatic aging.

Aging is commonly accompanied by a progressive decline of cellular functions, but the aging liver appears to preserve its function relatively well [9, 18, 19]. In this study, the aging-related alterations in the four omics were generally mild, although fat accumulation was clearly observed in the liver. Transcriptome analysis identified changed levels of cytochrome P450 family members, whereas proteome analysis found alterations of both cytochrome P450 and cytochrome c family member levels. However, cytochromes are involved in many metabolic processes of endogenous or exogenous compounds [20, 21]. Although aging is a risk factor for NAFLD [9, 22], lipid metabolism may not be the

critical pathway during hepatic aging. We, therefore, sought additional lines of evidence to further explore hepatic aging using acetylome and metabolome analyses.

Acetylation is a post-translational modification that integrates key physiological processes with gene regulation [23]. Acetylation is sensitive to intracellular metabolic alterations because acetyl-CoA derived from nutrient metabolism, especially lipid-derived acetyl-CoA, is its major carbon source [24]. The metabolome represents the collection of small molecules involved in metabolism, and improvements in the relevant analytical technologies provide significant information for biomarker and mechanism analyses [25, 26]. In this study, transcriptome, proteome, acetylome, and metabolome analyses each presented characteristic changes during aging. However, alterations in pyrimidine and glutathione metabolisms were especially notable because they were observed in all four omics results in the aging liver.

Down-regulation of nucleic acid metabolism occurs in *Caenorhabditis elegans* and mouse heart during aging [7, 27]. Intermediates of pyrimidine or purine metabolism, such as uridine, cytidine, and hypoxanthine, extend the lifespan of *C. elegans* [7, 28]. Our metabolome data identified increased levels of deoxycytidine, D-ribose 5-phosphate, AMP, and adenine, and decreased levels of dihydrofolate, dihydrouracil, deoxyuridine, uracil, cytidine, thymidine, xanthine, AICAR, IMP, and GMP in the aging mouse liver. Disruption of nucleic acid metabolism is associated with increased mutagenesis, genomic instability, and tumorigenesis. Alterations of intracellular deoxyribonucleoside triphosphate (dNTP) pools may impair DNA synthesis and DNA replication, causing cell cycle dysregulation and double-stranded DNA breaks [29–31]. During hepatic aging, we observed down-regulation of *Cdk1*, *Cdkn2c*, *Ccnd2* (cyclin D2), *Ccne2* (cyclin E2), *Ccnl1* (cyclin L1), *Ccnl2* (cyclin L2), and *Ccnt2* (cyclin T2), and up-regulation of *Inca1* (inhibitor of CDK, cyclin A1 interacting protein 1) in the transcriptome. In the proteome of the aging liver, we observed decreased levels of cyclin-dependent kinase inhibitor 1B (Cdkn1b). These changes in the levels of cell cycle-associated transcripts and proteins indicate that cell cycle dysregulation is likely to happen in the mouse liver during aging [32, 33], and may partially contribute to pyrimidine metabolism dysregulation. Moreover, down-regulation of histones, together with dysregulated pyrimidine metabolism, may exacerbate aging-associated genomic instability. Considering that the liver is the major organ for nucleic acid metabolism in mammals, a dysregulated pyrimidine metabolism in the liver is likely to change the levels of nucleic acids in the whole body and accelerate systemic aging.

The decrease in glutathione levels during aging was found decades ago [34, 35]. Glutathione deficiency increases the cellular risk for oxidative damage, and glutathione imbalance is observed in a wide range of pathological conditions [36]. In this study, however, metabolome analysis only identified decreased levels of glutathione disulfide, 5-L-glutamyl-L-alanine, gamma-L-glutamyl-L-valine, and gamma-L-glutamyl-L-glutamic acid in the aging mouse liver. We expect that improvements in metabolome technology may help to identify more metabolites and detect variations in glutathione levels directly in future studies.

This study also revealed that immunological function is altered during hepatic aging. Previous studies reported broadly up-regulated interferon signaling with aging across tissues and species [13, 14]. In this

multi-omics aging study, transcriptome analysis revealed up-regulated arachidonic acid metabolism, including prostamide/prostaglandin F synthase and leukotriene-B(4) omega-hydroxylase 2, during aging, and metabolome analysis confirmed increased arachidonic acid levels in the aging liver. In addition, the complement and coagulation cascades were decreased in both the transcriptome and proteome. Decreased complement may contribute to decreased hepatic protein synthesis ability and/or inflammation-associated complement consumption. As Xia *et al.* have summarized, aging-associated adaptive immunity decline is called immunosenescence, and an increase in the body's proinflammatory status with advancing age is called inflamm-aging [37, 38]. Thus, inflamm-aging and immunosenescence may simultaneously occur during hepatic aging.

Mammalian aging is a highly complex process spanning gene expression to metabolism, and thus multi-omics analysis can strongly support aging research. However, although each omics analysis provided abundant information, integrated analysis among them is quite a challenge. In this study, we pooled the liver samples and performed proteome and acetylome analyses using an MS2-based TMT strategy and the Significance A algorithm. MS2-based TMT can identify peptides precisely but introduce ratio compression [39]. We probably obtained a shortlist of differentially expressed proteins and excluded the interference of individual differences to some extent. We calculated Spearman correlation coefficients and found that the correlation between transcriptome and proteome and between proteome and acetylome were both low. Differences between each omics brought obstacles to reconstruct complete biological processes and signaling pathways but also prompted us to view aging from new perspectives. We expect technical and analytical improvements to increase identification accuracy and help future multi-omics analyses. We also hope that more omics methods can be applied and integrated for aging research. It is important to investigate other organs and both sexes in future studies to avoid biases [40] and obtain a comprehensive profile of liver aging and systematic aging.

Conclusions

In summary, we provide the first integrated transcriptome, proteome, acetylome, and metabolome profiling of mouse liver during normal aging, offering a comprehensive data resource for future aging research. The transcriptome, proteome, and acetylome profiles were clearly different in young and old livers, but metabolome profiles were not. Metabolic alterations in the mouse liver during aging were extremely complex, but dysregulated pyrimidine and glutathione metabolisms seemed notable. In addition, we found increased arachidonic acid metabolism and decreased complement and coagulation cascades in the aging mouse liver, suggesting that inflammatory and immune responses change during aging. Hepatic aging may contribute to systematic aging, may be a target for aging interventions, and deserves further exploration.

Methods

Animals

Wild-type C57BL/6 male mice were allowed to take food and water ad libitum. Colony rooms were maintained at a constant temperature and humidity with a 12:12 light/dark cycle. All animal protocols were approved by the Animal Care and Use Committee of the Institute of Basic Medical Sciences, Chinese Academy of Medical Sciences, and Peking Union Medical College.

Sample preparation

Two-month-old mice were defined as young and eighteen-month-old mice as old. Mice were sacrificed by massive bloodletting from the orbital vessels after anesthesia with tribromoethanol. Next, the whole liver was detached from each mouse, immediately dissected, and stored separately. Samples acquired for metabolome, transcriptome, proteome, and acetylome analyses were immediately frozen in liquid nitrogen and transferred to -80 ℃ until use. Samples for H & E and Masson analyses were quickly placed in 4% paraformaldehyde (PFA). Samples for oil red O analysis were appropriately embedded into optimal cutting temperature compound (OCT) and stored at -80 ℃ until use.

Morphological analysis

H & E and Masson staining

Liver samples were fixed in 4% PFA overnight. Fixed tissues were dehydrated by placing in 75% ethanol for 4 h, followed by 85% ethanol for 2 h, 90% ethanol for 2 h, 95% ethanol for 1 h, absolute ethanol for 30 min twice, ethanol-dimethylbenzene for 5 min, and dimethylbenzene twice for 10 min. Dehydrated tissues were embedded in paraffin and cut into 4 μm-thick sections. The paraffin-embedded sections were successively placed in dimethylbenzene twice for 20 min each, absolute ethanol for 10 min twice, 95% ethanol for 5 min, 90% ethanol for 5 min, 80% ethanol for 5 min, 70% ethanol for 5 min, and washed with distilled water.

For H & E staining, hydrated sections were placed in hematoxylin solution for 3–8 min, 1% hydrochloric acid/ethanol differentiation solution for seconds, 0.6% ammonia for seconds, and eosin solution for 1–3 min.

For Masson staining, hydrated sections were processed according to the manufacturer's protocol of the Masson staining kit (Wuhan Goodbio Technology Co., Ltd, G1006).

Stained sections were subsequently transferred into 95% ethanol for 5 min twice, absolute ethanol for 5 min twice, and dimethylbenzene for 5 min twice. Next, the sections were dried and sealed with neutral gum. Pictures were taken with a Nikon Eclipse CI imaging system.

Oil Red O staining

Liver samples embedded in OCT were moved to a freezing microtome and cut into 8 μm-thick sections at -20 ℃. The sections were dried at room temperature for 10 min, fixed with 4% paraformaldehyde (PFA) for 15 min, and washed with phosphate-buffered saline (PBS) for 5 min three times. Sections were transferred into oil red O solution (G1016, Goodbio Technology Co., Ltd) for 10 min, followed by 75%

ethanol for 2 s, and then washed with water for 1 min. Next, the sections were transferred to hematoxylin solution for 1 min, 1% hydrochloric acid/ethanol differentiation solution for 3 s, and 0.6% ammonia for 3 s, after which they were washed with water. Excess water was removed, and glycerin gelatin was used to seal the sections. Pictures were taken using a Nikon Eclipse CI imaging system (Japan).

RNA sequencing and analysis

RNA isolation, library preparation, and sequencing were performed by Novogene Bioinformatics Technology Co., Ltd (Tianjin, China). Briefly, a total of 3 μg RNA per sample was used as input material for RNA sample preparation. First, ribosomal RNA was removed with the Epicentre Ribo-zero™ rRNA Removal Kit (RZH1046, Epicentre, USA), and rRNA free residue was cleaned up by ethanol precipitation. Subsequently, sequencing libraries were generated using the rRNA-depleted RNA by NEBNext® Ultra™ Directional RNA Library Prep Kit for Illumina® (NEBE7770, NEB, USA) following the manufacturer's recommendations. Fragmentation was carried out using divalent cations under elevated temperature in NEBNext First-Strand Synthesis Reaction Buffer (5×). First-strand cDNA was synthesized using random hexamer primer and M-MuLV Reverse Transcriptase (RNase H). Second strand cDNA synthesis was subsequently performed using DNA Polymerase I and RNase H. In the reaction buffer, dTTP was replaced by dUTP. Remaining overhangs were converted into blunt ends via exonuclease/polymerase activities. After adenylation of 3' ends of DNA fragments, NEBNext Adapter with hairpin loop structure was ligated to prepare for hybridization. To select cDNA fragments of preferentially 150 ~ 200 bp in length, library fragments were purified with AMPure XP system (Beckman Coulter, Beverly, USA). Next, 3 μL USER Enzyme (NEB, USA) was used with size-selected, adaptor-ligated cDNA at 37 ℃ for 15 min, followed by 5 min at 95 ℃ before PCR. PCR was performed with Phusion High-Fidelity DNA polymerase, Universal PCR primers, and Index (X) Primer. At last, products were purified (AMPure XP system), and library quality was assessed on an Agilent Bioanalyzer 2100 system. Clustering of the index-coded samples was performed on a cBot Cluster Generation System using TruSeq PE Cluster Kit v3-cBot-HS (Illumina) according to the manufacturer's instructions. After cluster generation, the libraries were sequenced on an Illumina HiSeq 4000 instrument, and 150 base pair and paired-end reads were generated. For quality control, raw data in fastq format were first processed using Novogene Perl scripts. Clean data were obtained by removing reads containing adapters, reads containing poly-N, and low-quality reads from the raw data. In addition, the Q20, Q30, and GC contents of the clean data were calculated. All downstream analyses were based on the clean data with high quality. RNA sequencing data were deposited in the Sequence Read Archive under the BioProject ID PRJNA609589.

Reference genome and gene model annotation files were downloaded from the Ensembl website (genome: ftp://ftp.ensembl.org/pub/release-97/fasta/mus_musculus/dna/Mus_musculus.GRCm38.dna.primary_assembly.fa.gz; gtf: ftp://ftp.ensembl.org/pub/release-97/gtf/mus_musculus/Mus_musculus.GRCm38.97.gtf.gz). HISAT2 (v2.0.5) was used to build the reference genome index and align paired-end clean reads to the reference genome. Then, StringTie (v1.3.3) was used to assemble the mapped reads of each sample and calculate FPKMs of coding genes. FPKM means fragments per kilo-base of exon per million fragments mapped,

calculated based on the length of the fragments, and reads count mapped to this fragment. Transcripts with FPKM values > 1 in over 50% of the samples in either group were considered validated. The edgeR R package (v3.243) provided statistical routines for determining differential expression in digital transcript or gene expression data using a model based on a negative binomial distribution. Transcripts with adjusted p-values < 0.05 were considered to be differentially expressed. Up- and down-regulated transcripts were determined based on the log2 fold-change (FC) (generated by edgeR, old mice/young mice) > 0 or < 0, respectively.

Proteome and acetylome analyses

Protein extraction

Samples stored in -80 ℃ were separately ground into a powder after submersion in liquid nitrogen and transferred to individual 5-mL centrifuge tubes. Four volumes of lysis buffer (8 M urea, 2 mM ethylenediaminetetraacetic acid (EDTA), 3 μM trichostatin A, 50 mM nicotinamide, 10 mM dithiothreitol, and 1% Protease Inhibitor Cocktail) were added to the cell powder, followed by sonication for three times on ice using a high-intensity ultrasonic processor. Cell debris was removed by centrifugation at 12,000 × *g* at 4 ℃ for 10 min. Each supernatant was collected, and protein concentrations were determined with a BCA Kit (P0011, Beyotime, Shanghai, China) according to the manufacturer's instructions. Total protein samples were split into four groups and then pooled into Young 1 (1–7 of young mice), Young 2 (8–14 of young mice), Old 1 (1–5 of old mice), and Old 2 (6–10 of old mice) groups.

Protein digestion

For digestion, 3.7 mg protein was reduced with 5 mM dithiothreitol for 30 min at 56 ℃ and alkylated with 11 mM iodoacetamide for 15 min at room temperature in the dark. The protein sample was then diluted by adding 100 mM triethylammonium bicarbonate (TEAB) to less than 2 M urea. Next, trypsin (V5280, Promega, Madison, WI, USA) was added at a 1:50 trypsin-to-protein mass ratio for the first digestion overnight and a 1:100 trypsin-to-protein mass ratio for a second digestion for 4 h.

Tandem mass tag (TMT) labeling

After trypsin digestion, peptides were desalted using a Strata X C18 SPE column (Phenomenex, Torrance, CA, USA) and vacuum-dried. Peptides were reconstituted in 0.5 M TEAB and processed according to the manufacturer's instructions for TMT labeling (90068, Thermo Fisher Scientific, Rockford, IL, USA). Briefly, one unit of TMT reagent was thawed and reconstituted in ACN. Peptide mixtures were then incubated for 2 h at room temperature and pooled, desalted, and dried by vacuum centrifugation.

High pH reversed-phase pre-fractionation of peptides

TMT labeled peptides (10% for proteome analysis, and the remaining 90% for acetylome analysis) were fractionated by high pH reversed-phase high-performance liquid chromatography. For proteome analysis, a 300 Extend C18 column (5 μm particles, 4.6 mm inside diameter [ID], and 250 mm length; Agilent) was used. Peptides were separated into 60 fractions by stepwise increases in ACN concentration (8–32% in

60 min, 1 mL/min) at pH 9.0. Total fractions were split into nine groups and then pooled and vacuum-dried. For acetylome analysis, a Betasil C18 column (5 μm particles, 10 mm ID, and 250 mm length; Thermo Fisher Scientific) was used. The gradient and mobile phase times were the same as those used for the proteome. The obtained 60 fractions were split into four groups, pooled, and vacuum-dried.

Acetylated peptide enrichment

To enrich for acetylated peptides, pre-fractionated peptides for acetylomics analysis were dissolved in NETN buffer (100 mM NaCl, 1 mM EDTA, 50 mM Tris-HCl, 0.5% NP-40, pH 8.0) and incubated overnight at 4 °C with 20 μL pre-washed antibody beads (PTM104, PTM Biolabs, Hangzhou, China) with gentle shaking. Beads were washed four times with NETN buffer and twice with H_2O. Bound peptides were eluted from the beads with 0.1% trifluoroacetic acid, desalted, and vacuum-dried.

Liquid chromatography (LC) tandem mass spectrometry (MS) analysis of peptide mixtures

A Q Exactive™ HF-X mass spectrometer interfaced with an EASY-nLC 1200 nanoflow LC system (Thermo Fisher Scientific) was used for LC-MS analysis. Samples for proteome and acetylome analysis were separately resuspended in mobile phase A (0.1% formic acid and 2% ACN in water) and loaded onto the EASY-nLC 1200 nanoflow LC system at a constant flow rate of 400 nL/min. Mobile phase B contained 0.1% formic acid and 90% ACN in water. For proteome analysis, the following gradient was used: 8%-22% B for 0–38 min, 22%-32% B for 38–52 min, 32–80% B for 52–56 min, and 80% B for 56–60 min. For acetylome analysis, the following gradient was used: 9%-23% B for 0–24 min, 23%-35% B for 24–32 min, 35%-80% B for 32–36 min, and 80% B for 36–40 min. For proteome analysis, a data-dependent strategy was used by first obtaining MS1 data in the Orbitrap at a resolution of 120,000 (at an m/z ratio of 200 and a maximum injection time of 50 ms for target values of 3e6 ions in the 350–1600 m/z mass range). For the MS2 scan, the top 30 precursor ions (charge state from + 2 to + 5) were selected for fragmentation by higher-energy collision dissociation with a normalized collision energy (NCE) of 28%. A total of 5e4 ions were accumulated over 40 ms as the maximum permitted filling time for each scan. Dynamic exclusion time was set to 30 s to reduce the repeated fragmentation of precursor ions. For acetylome analysis, the data-dependent strategy was also used. MS1 was measured in the Orbitrap at a resolution of 120,000 (at an m/z ratio of 200 and a maximum injection time of 50 ms for target values of 3e6 ions in the 350–1600 m/z mass range). For MS2 scan, the top 20 precursor ions (charge state from + 2 to + 5) were selected for fragmentation by higher-energy collision dissociation with an NCE of 28%. A total of 1e5 ions were accumulated over 100 ms as the maximum permitted filling time for each scan. Dynamic exclusion time was set to 10 s.

Database searches

Raw MS/MS data were analyzed using the MaxQuant search engine (v.1.5.2.8) [41] against the Swiss-Prot Mouse database (updated on June 24, 2019; 17,014 entries) concatenated with the reverse decoy database. Trypsin/P was specified as the cleavage enzyme. Two missing cleavages were allowed for proteome analysis, and four missing cleavages were allowed for acetylome analysis. The mass tolerance

for precursor ions was set to 20 ppm in the first search or 5 ppm in the main search, and the mass tolerance of fragment ions was set to 0.02 Da. A carbamidomethyl group on a Cys residue was specified as a fixed modification. Oxidation of Met and protein N-terminal acetylation were set as variable modifications for proteome analysis, and acetylation of Lys, oxidation of Met, and protein N-terminal acetylation were set as variable modifications for acetylome analysis. The false discovery rate (FDR) was adjusted to < 1%, and the minimum score for modified peptides was set to > 40. The MS-proteomics data were deposited in the ProteomeXchange Consortium via the iProX partner repository [42] under the dataset identifier PXD018003 (subproject ID of proteome: IPX0002001001; subproject ID of acetylome: IPX0002001002).

Data management

Proteins/peptides in the reverse decoy database and potential contaminant database were excluded for both proteomics and acetylomics analyses. In addition, the localization probability of acetylation in the acetylome ranged from 0 to 1. Peptides with localization probabilities of > 0.75 were grouped into Class I and were selected for further analysis. Normalization of the proteome and acetylome data was performed with Perseus (v.1.6.5.0) [43] by dividing the intensity by the median of each group. Significance A analysis was performed using Perseus, and a protein/site with Benjamini-Hochberg FDR < 0.05 was considered differentially expressed [41, 43]. Up- and down-regulated proteins/peptides were determined as FC (mean values of old mice/mean values of young mice) > 1 or < 1, respectively.

Functional enrichment analysis

Kyoto Encyclopedia of Genes and Genomes (KEGG) [44] enrichment analysis was performed using KOBAS [45]. We chose the hypergeometric test/Fisher's exact test as the statistical method and QVALUE as the FDR correction method. KEGG terms with a corrected p-value of < 0.05 were considered as significantly enriched.

Motif analysis

To obtain the sequence characteristics of acetylated peptides, Class I acetylated peptides were submitted to MoMo modification motifs (http://meme-suite.org/tools/momo) [46] for motif analysis using the motif-x algorithm.

Metabolome analysis

Sample preparation, LC-MS analysis, peak extraction, and compound identification were performed in Dr. Zheng-Jiang Zhu's laboratory, as previously described [47]. Briefly, 20 mg tissue per liver sample was homogenized with 200 μL H_2O using cooled nitrogen gas flow from liquid nitrogen. Each 200 μL homogenate solution was mixed with 800 μL methanol/acetonitrile (volume ratio, 1:1) and incubated for 1 h at -20 ℃. Afterward, the samples were centrifuged for 15 min at 13,000 rpm and 4 ℃. The supernatants were evaporated to dryness at 4 ℃ using a vacuum concentrator. Then, each sample was reconstituted with 100 μL acetonitrile/H_2O (volume ratio, 1:1) and centrifuged for 15 min at 13,000 rpm and 4 ℃. The samples were stored at -80 ℃ before LC-MS analysis.

For liquid chromatography, a Waters ACQUITY UPLC BEH Amide column (1.7 μm particles, 2.1 mm ID, and 100 mm length) was used. Mobile phase A was 25 mM ammonium acetate and 25 mM ammonium hydroxide in 100% water (pH 9.6), and mobile phase B was 100% acetonitrile (ACN). The following linear gradient was used for elution: 95% B (0.0–1.0 min), 95% B to 65% B (1.0–14.0 min), 65% B to 40% B (14.0–16.0 min), 40% B (16.0–18.0 min), 40% B to 95% B (18.0-18.1 min), and 95% B for 4.9 min. The flow rate was 0.30 mL/min, and the sample injection volume was

2 μL.

A TripleTOF 6600 mass spectrometer (AB Sciex) was used for information-dependent acquisition (IDA) of MS/MS spectra. In IDA mode, the acquisition software (Analyst TF 1.7, AB Sciex) continuously evaluated the full-scan survey of MS data as it was collected and triggered the acquisition of MS/MS spectra depending on predefined criteria. In each cycle, the most intensive 12 precursor ions with a signal intensity above 100 were chosen for MS/MS at a collision energy of 30 eV. The cycle time was 0.56 s. The following electrospray ionization conditions were used: ion source gas 1, 60 pounds per square inch (psi); ion source gas 2, 60 psi; curtain gas, 35 psi; source temperature, 600 ℃; declustering potential, 60 V; ion spray voltage floating, 5000 V or -4000 V in positive or negative mode, respectively. The data obtained in positive-ion mode (POS) and negative-ion mode (NEG) were separately submitted for informatics analysis.

Raw data in wiff format were analyzed using an in-house software program developed in Dr. Zheng-Jiang Zhu's laboratory to perform peak extraction and compound quantification. Peaks appearing in over 50% of all samples were considered to represent true feature hits. The mass error tolerance for MS1 matches was set to ± 25 ppm, and the mass error tolerance for MS2 matches was set to ± 35 ppm. MS2 spectral similarity scores were set to range from 0 to 1, and compounds with a score of > 0.6 were further analyzed.

Data management was initially implemented by Shanghai Biotree Biotech Co., Ltd. Briefly, missing values were inserted as half of the minimum value, and the data were normalized by the total ion current. The collated data were entered into the SIMCA14 software program (v14.1, Sartorius Stedim Data Analytics AB, Umea, Sweden) for supervised orthogonal projections to latent structures-discriminate analysis (OPLS-DA), and the first principal component of variable importance in the projection (VIP) was obtained. FC (mean values of old mice/mean values of young mice) was calculated, and Student's *t*-test was used to determine p-values. Compounds with both a VIP > 1 and a p-value < 0.05 were preliminarily selected as differentially expressed metabolites and as candidates for pathway analysis.

Compounds identified in POS and NEG mode were combined to obtain the overall set. For compounds identified in both POS and NEG mode, those with higher MS2 spectrum similarity scores were retained if they displayed consistent changing trends, whereas those with contradictory FC were discarded. Up- and down-regulated compounds were determined as those with FC > 1 or < 1, respectively. An arranged compound dataset was submitted to the MetaboAnalyst website (https://www.metaboanalyst.ca/) [48, 49] for pathway analysis (over-representation analysis: Fisher's exact test; pathway topology analysis:

relative-betweenness centrality; pathway library: Mus musculus KEGG). The MS-based metabolomics data were deposited in the ProteomeXchange Consortium under the dataset identifier PXD018003 (subproject ID: IPX0002001003).

Abbreviations

ER Endoplasmic reticulum

FC Fold-change

FDR False discovery rate

ID Inside diameter

IDA Information-dependent acquisition

IPA Ingenuity Pathway Analysis

KEGG Kyoto Encyclopedia of Genes and Genomes

LC Liquid chromatography

MS Mass spectrometry

NCE Normalized collision energy

OCT Optimal cutting temperature

PBS Phosphate-buffered saline

PCA Principal component analysis

QC Quality control

TMT Tandem mass tag

VIP Variable importance in the projection

Declarations

Ethics approval and consent to participate

All animal protocols were approved by the Animal Care and Use Committee of the Institute of Basic Medical Sciences, Chinese Academy of Medical Sciences, and Peking Union Medical College.

Consent for publication

Not applicable

Competing interests

The authors declare that they have no competing interests.

Availability of data and materials

Raw proteome, acetylome, and metabolome data are deposited in the ProteomeXchange Consortium under the dataset identifier PXD018003. Raw transcriptome data are deposited in the Sequence Read Archive under the BioProject ID PRJNA609589.

Competing interests

The authors declare that there are no conflicts of interest.

Funding

This work was supported by grants from the Chinese Academy of Medical Sciences Innovation Fund for Medical Sciences [grant numbers CIFMS2017-I2M-1-008 and CIFMS2019-I2M-1-004].

Author's contributions

J.Y. and H.C. conceived and designed the project. J.L. and S.W. performed the analyses. J.L., J.Y., and C.L. wrote the manuscript. All authors reviewed and approved the final manuscript.

Acknowledgement

We thank members of the De-Pei Liu laboratory and Zheng-Jiang Zhu laboratory for helpful discussions regarding this project.

References

1. Lopez-Otin C, Blasco MA, Partridge L, Serrano M, Kroemer G. The hallmarks of aging. Cell. 2013; 153(6):1194-1217.
2. Partridge L, Deelen J, Slagboom PE. Facing up to the global challenges of ageing. Nature. 2018; 561(7721):45-56.
3. Zhang W, Qu J, Liu GH, Belmonte JCI. The ageing epigenome and its rejuvenation. Nat Rev Mol Cell Biol. 2020.
4. Campisi J, Kapahi P, Lithgow GJ, Melov S, Newman JC, Verdin E. From discoveries in ageing research to therapeutics for healthy ageing. Nature. 2019; 571(7764):183-192.
5. White RR, Milholland B, MacRae SL, Lin M, Zheng D, Vijg J. Comprehensive transcriptional landscape of aging mouse liver. BMC Genomics. 2015; 16:899.

6. Walther DM, Mann M. Accurate quantification of more than 4000 mouse tissue proteins reveals minimal proteome changes during aging. Mol Cell Proteomics. 2011; 10(2):M110 004523.
7. Copes N, Edwards C, Chaput D, Saifee M, Barjuca I, Nelson D, Paraggio A, Saad P, Lipps D, Stevens SM, Jr. *et al*. Metabolome and proteome changes with aging in Caenorhabditis elegans. Exp Gerontol. 2015; 72:67-84.
8. He X, Memczak S, Qu J, Belmonte JCI, Liu G-H. Single-cell omics in ageing: a young and growing field. Nature Metabolism. 2020; 2(4):293-302.
9. Tajiri K, Shimizu Y. Liver physiology and liver diseases in the elderly. World J Gastroenterol. 2013; 19(46):8459-8467.
10. Morsiani C, Bacalini MG, Santoro A, Garagnani P, Collura S, D'Errico A, de Eguileor M, Grazi GL, Cescon M, Franceschi C *et al*. The peculiar aging of human liver: A geroscience perspective within transplant context. Ageing Res Rev. 2019; 51:24-34.
11. Bacalini MG, Franceschi C, Gentilini D, Ravaioli F, Zhou X, Remondini D, Pirazzini C, Giuliani C, Marasco E, Gensous N *et al*. Molecular Aging of Human Liver: An Epigenetic/Transcriptomic Signature. J Gerontol A Biol Sci Med Sci. 2019; 74(1):1-8.
12. Horvath S, Erhart W, Brosch M, Ammerpohl O, von Schonfels W, Ahrens M, Heits N, Bell JT, Tsai PC, Spector TD *et al*. Obesity accelerates epigenetic aging of human liver. Proc Natl Acad Sci U S A. 2014; 111(43):15538-15543.
13. Benayoun BA, Pollina EA, Singh PP, Mahmoudi S, Harel I, Casey KM, Dulken BW, Kundaje A, Brunet A. Remodeling of epigenome and transcriptome landscapes with aging in mice reveals widespread induction of inflammatory responses. Genome Res. 2019; 29(4):697-709.
14. Kim Y, Kwon OK, Chae S, Jung HJ, Ahn S, Jeon JM, Sung E, Kim S, Ki SH, Chung KW *et al*. Quantitative Proteomic Analysis of Changes Related to Age and Calorie Restriction in Rat Liver Tissue. Proteomics. 2018; 18(5-6):e1700240.
15. Sato S, Solanas G, Peixoto FO, Bee L, Symeonidi A, Schmidt MS, Brenner C, Masri S, Benitah SA, Sassone-Corsi P. Circadian Reprogramming in the Liver Identifies Metabolic Pathways of Aging. Cell. 2017; 170(4):664-677 e611.
16. Bochkis IM, Przybylski D, Chen J, Regev A. Changes in nucleosome occupancy associated with metabolic alterations in aged mammalian liver. Cell Rep. 2014; 9(3):996-1006.
17. Ogrodnik M, Miwa S, Tchkonia T, Tiniakos D, Wilson CL, Lahat A, Day CP, Burt A, Palmer A, Anstee QM *et al*. Cellular senescence drives age-dependent hepatic steatosis. Nat Commun. 2017; 8:15691.
18. Hunt NJ, Kang SWS, Lockwood GP, Le Couteur DG, Cogger VC. Hallmarks of Aging in the Liver. Comput Struct Biotechnol J. 2019; 17:1151-1161.
19. Anantharaju A, Feller A, Chedid A. Aging Liver. A review. Gerontology. 2002; 48(6):343-353.
20. Santucci R, Sinibaldi F, Cozza P, Polticelli F, Fiorucci L. Cytochrome c: An extreme multifunctional protein with a key role in cell fate. Int J Biol Macromol. 2019; 136:1237-1246.

21. Guengerich FP. Cytochrome P450 research and The Journal of Biological Chemistry. J Biol Chem. 2019; 294(5):1671-1680.
22. Gong Z, Tas E, Yakar S, Muzumdar R. Hepatic lipid metabolism and non-alcoholic fatty liver disease in aging. Mol Cell Endocrinol. 2017; 455:115-130.
23. Menzies KJ, Zhang H, Katsyuba E, Auwerx J. Protein acetylation in metabolism - metabolites and cofactors. Nat Rev Endocrinol. 2016; 12(1):43-60.
24. McDonnell E, Crown SB, Fox DB, Kitir B, Ilkayeva OR, Olsen CA, Grimsrud PA, Hirschey MD. Lipids Reprogram Metabolism to Become a Major Carbon Source for Histone Acetylation. Cell Rep. 2016; 17(6):1463-1472.
25. Rinschen MM, Ivanisevic J, Giera M, Siuzdak G. Identification of bioactive metabolites using activity metabolomics. Nat Rev Mol Cell Biol. 2019; 20(6):353-367.
26. Johnson CH, Ivanisevic J, Siuzdak G. Metabolomics: beyond biomarkers and towards mechanisms. Nat Rev Mol Cell Biol. 2016; 17(7):451-459.
27. Brink TC, Demetrius L, Lehrach H, Adjaye J. Age-related transcriptional changes in gene expression in different organs of mice support the metabolic stability theory of aging. Biogerontology. 2009; 10(5):549-564.
28. Wan QL, Meng X, Fu X, Chen B, Yang J, Yang H, Zhou Q. Intermediate metabolites of the pyrimidine metabolism pathway extend the lifespan of C. elegans through regulating reproductive signals. Aging (Albany NY). 2019; 11(12):3993-4010.
29. Kim J, Hu Z, Cai L, Li K, Choi E, Faubert B, Bezwada D, Rodriguez-Canales J, Villalobos P, Lin YF *et al*. CPS1 maintains pyrimidine pools and DNA synthesis in KRAS/LKB1-mutant lung cancer cells. Nature. 2017; 546(7656):168-172.
30. Poli J, Tsaponina O, Crabbe L, Keszthelyi A, Pantesco V, Chabes A, Lengronne A, Pasero P. dNTP pools determine fork progression and origin usage under replication stress. EMBO J. 2012; 31(4):883-894.
31. Wang X, Yang K, Wu Q, Kim LJY, Morton AR, Gimple RC, Prager BC, Shi Y, Zhou W, Bhargava S *et al*. Targeting pyrimidine synthesis accentuates molecular therapy response in glioblastoma stem cells. Sci Transl Med. 2019; 11(504).
32. Lemmens B, Lindqvist A. DNA replication and mitotic entry: A brake model for cell cycle progression. J Cell Biol. 2019; 218(12):3892-3902.
33. Pack LR, Daigh LH, Meyer T. Putting the brakes on the cell cycle: mechanisms of cellular growth arrest. Curr Opin Cell Biol. 2019; 60:106-113.
34. Hazelton GA, Lang CA. Glutathione contents of tissues in the aging mouse. Biochem J. 1980; 188(1):25-30.
35. Hazelton GA, Lang CA. Glutathione peroxidase and reductase activities in the aging mouse. Mech Ageing Dev. 1985; 29(1):71-81.

36. Teskey G, Abrahem R, Cao R, Gyurjian K, Islamoglu H, Lucero M, Martinez A, Paredes E, Salaiz O, Robinson B *et al*. Glutathione as a Marker for Human Disease. Adv Clin Chem. 2018; 87:141-159.
37. Xia S, Zhang X, Zheng S, Khanabdali R, Kalionis B, Wu J, Wan W, Tai X. An Update on Inflamm-Aging: Mechanisms, Prevention, and Treatment. J Immunol Res. 2016; 2016:8426874.
38. Salminen A, Huuskonen J, Ojala J, Kauppinen A, Kaarniranta K, Suuronen T. Activation of innate immunity system during aging: NF-kB signaling is the molecular culprit of inflamm-aging. Ageing Res Rev. 2008; 7(2):83-105.
39. Hogrebe A, von Stechow L, Bekker-Jensen DB, Weinert BT, Kelstrup CD, Olsen JV. Benchmarking common quantification strategies for large-scale phosphoproteomics. Nat Commun. 2018; 9(1):1045.
40. Mitchell SJ, Madrigal-Matute J, Scheibye-Knudsen M, Fang E, Aon M, Gonzalez-Reyes JA, Cortassa S, Kaushik S, Gonzalez-Freire M, Patel B *et al*. Effects of Sex, Strain, and Energy Intake on Hallmarks of Aging in Mice. Cell Metab. 2016; 23(6):1093-1112.
41. Cox J, Mann M. MaxQuant enables high peptide identification rates, individualized p.p.b.-range mass accuracies and proteome-wide protein quantification. Nat Biotechnol. 2008; 26(12):1367-1372.
42. Ma J, Chen T, Wu S, Yang C, Bai M, Shu K, Li K, Zhang G, Jin Z, He F *et al*. iProX: an integrated proteome resource. Nucleic Acids Res. 2019; 47(D1):D1211-D1217.
43. Tyanova S, Temu T, Sinitcyn P, Carlson A, Hein MY, Geiger T, Mann M, Cox J. The Perseus computational platform for comprehensive analysis of (prote)omics data. Nat Methods. 2016; 13(9):731-740.
44. Kanehisa M, Araki M, Goto S, Hattori M, Hirakawa M, Itoh M, Katayama T, Kawashima S, Okuda S, Tokimatsu T *et al*. KEGG for linking genomes to life and the environment. Nucleic Acids Res. 2008; 36(Database issue):D480-484.
45. Xie C, Mao X, Huang J, Ding Y, Wu J, Dong S, Kong L, Gao G, Li CY, Wei L. KOBAS 2.0: a web server for annotation and identification of enriched pathways and diseases. Nucleic Acids Res. 2011; 39(Web Server issue):W316-322.
46. Cheng A, Grant CE, Noble WS, Bailey TL. MoMo: discovery of statistically significant post-translational modification motifs. Bioinformatics. 2018; 35(16):2774-2782.
47. Zha H, Cai Y, Yin Y, Wang Z, Li K, Zhu ZJ. SWATHtoMRM: Development of High-Coverage Targeted Metabolomics Method Using SWATH Technology for Biomarker Discovery. Anal Chem. 2018; 90(6):4062-4070.
48. Chong J, Xia J. MetaboAnalystR: an R package for flexible and reproducible analysis of metabolomics data. Bioinformatics. 2018; 34(24):4313-4314.
49. hong J, Soufan O, Li C, Caraus I, Li S, Bourque G, Wishart DS, Xia J. MetaboAnalyst 4.0: towards more transparent and integrative metabolomics analysis. Nucleic Acids Res. 2018; 46(W1):W486-W494.

Figures

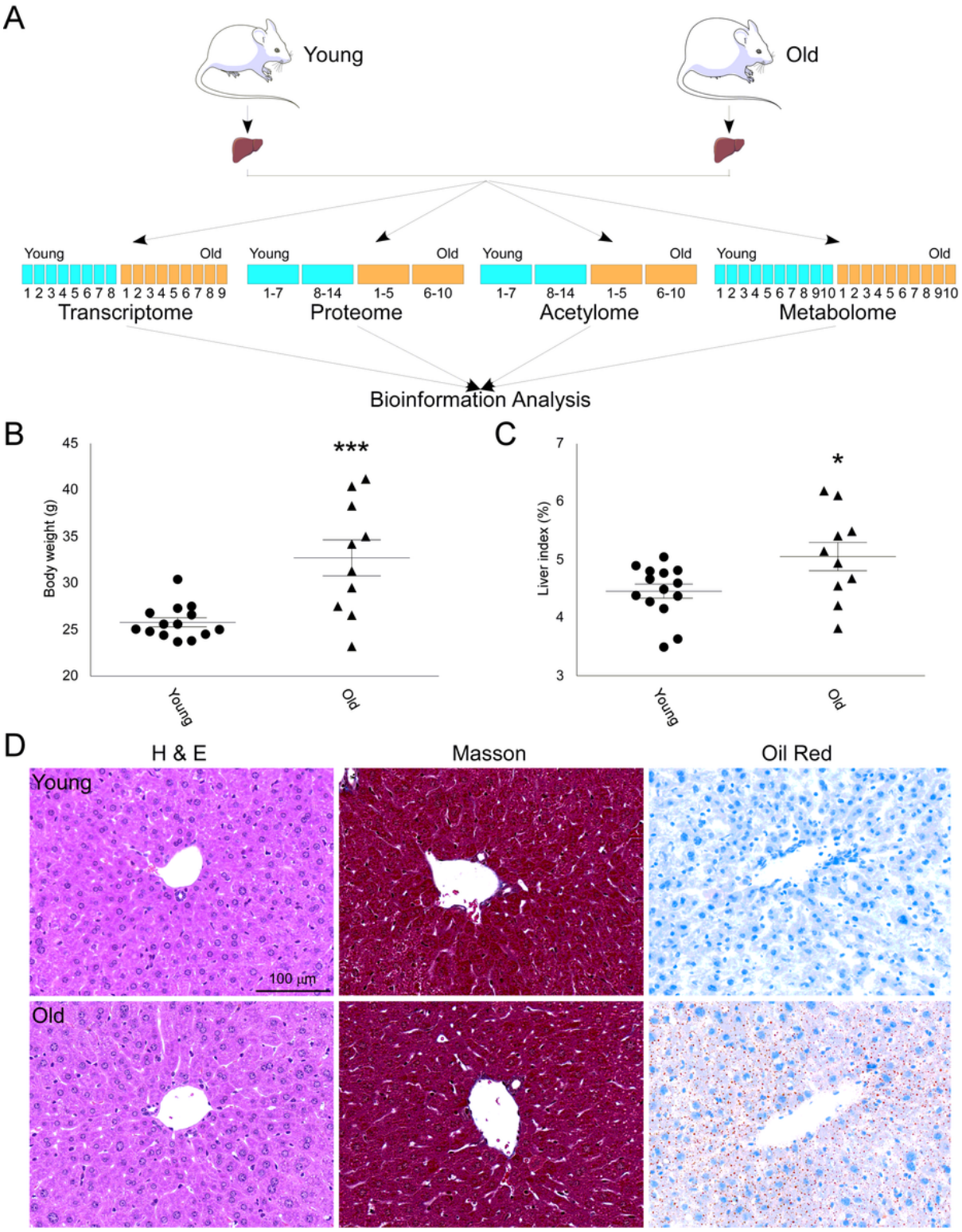

Figure 1

Mouse phenotype during normal aging. (A) Brief workflow of multi-omics analysis. The 2-month-old mice were defined as young and 18-month-old mice as old. Transcriptome and metabolome analyses were performed using individual liver samples. Proteome and acetylome analyses were performed using pooled samples. The number of mice is shown in the figure. (B) Bodyweight of mice (young: n =14; old: n = 10; mean ± standard error of the mean shown; ***t-test, $p < 0.001$). (C) Liver index of mice (young: n =

14; old: n = 10; mean ± standard error of the mean shown; *t-test, p < 0.05). (D) Morphological analysis of young and old mouse livers. Left panel: H & E staining. Middle panel: Masson staining. Right panel: oil red O staining.

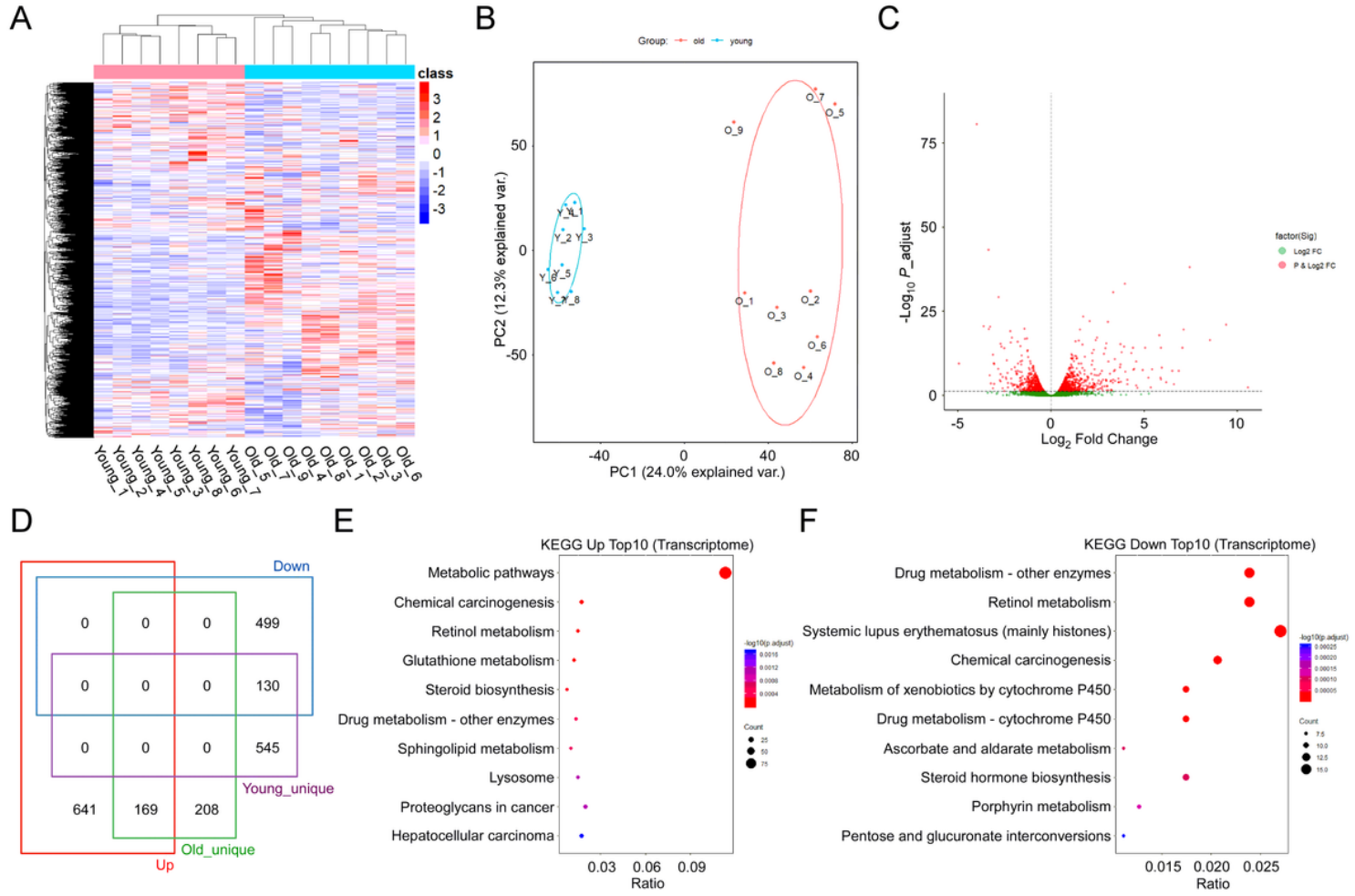

Figure 2

Hepatic transcriptome of young and old mice. (A) Hierarchical clustering analysis of young and old livers (transcripts with over 50% FPKM > 1 in at least one age group were used; clustering distance = Euclidean). (B) PCA of young and old livers. (C) Volcano plot of transcripts with over 50% FPKM > 1 in at least one age group. (D) Venn diagram of up-regulated, down-regulated, old-unique, and young-unique transcripts. Up: transcripts with over 50% FPKM > 1 in at least one group; edgeR adjusted p-value < 0.05 and log2 FC > 0. Down: transcripts with over 50% FPKM > 1 in at least one group; edgeR adjusted p-values < 0.05 and log2 FC < 0. Transcripts with over 50% FPKM > 1 in the young mice but less than 50% FPKM > 1 in the old mice as Young_unique, and transcripts with the contrary feature were considered as Old_unique. (E) Top 10 enriched KEGG pathways in up-regulated transcripts during aging. (F) Top 10 enriched KEGG pathways in down-regulated transcripts during aging.

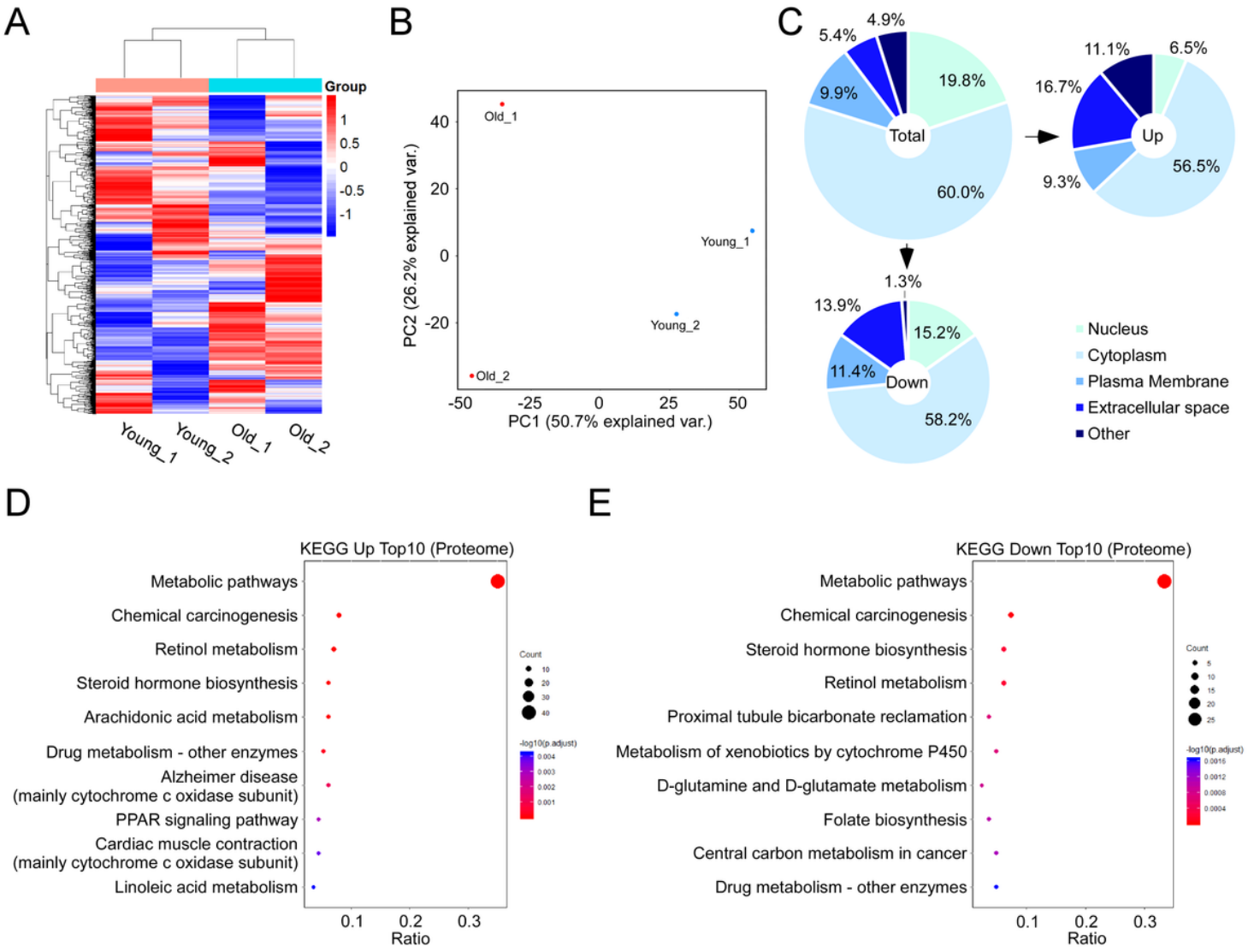

Figure 3

Hepatic proteome of young and old mice. (A) Hierarchical clustering analysis of young and old livers (4,712 quantifiable proteins were used; clustering distance = Euclidean). (B) PCA of young and old livers. (C) Location of the total, up-, and down-regulated proteins. Total: 4,712 quantifiable proteins. Up: 114 up-regulated proteins. Down: 81 down-regulated proteins. (D) Top 10 enriched KEGG pathways in up-regulated proteins during aging. (E) Top 10 enriched KEGG pathways in down-regulated proteins during aging.

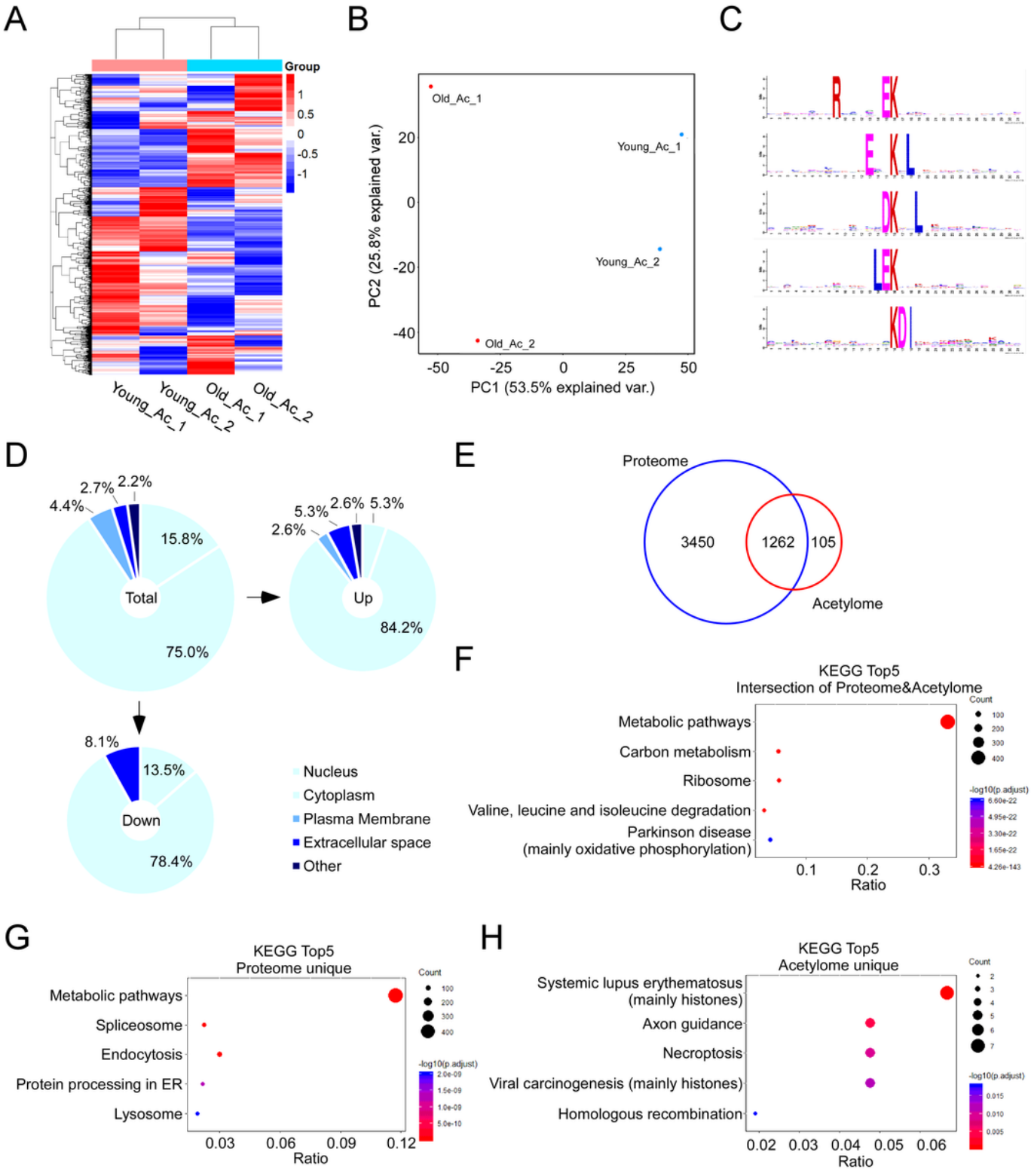

Figure 4

Hepatic acetylome of young and old mice. (A) Hierarchical clustering analysis of young and old livers (4,818 quantifiable Class I acetylated sites were used; clustering distance = Euclidean). (B) PCA of young and old livers. (C) Motif analysis of all 4,818 sequences with Class I acetylated sites. Top five identified motifs are listed. (D) Location analysis of the acetylated proteins. Total: All 1,367 acetylated proteins. Up: proteins with up-regulated acetylated sites. Down: proteins with down-regulated acetylated sites. (E) Venn

diagram of all quantifiable proteins in the proteome and all acetylated proteins in the acetylome. (F) Top 5 enriched KEGG pathways in proteins identified in both the proteome and acetylome. (G) Top 5 enriched KEGG pathways in proteins only identified in the proteome. (H) Top 5 enriched KEGG pathways in proteins only identified in the acetylome.

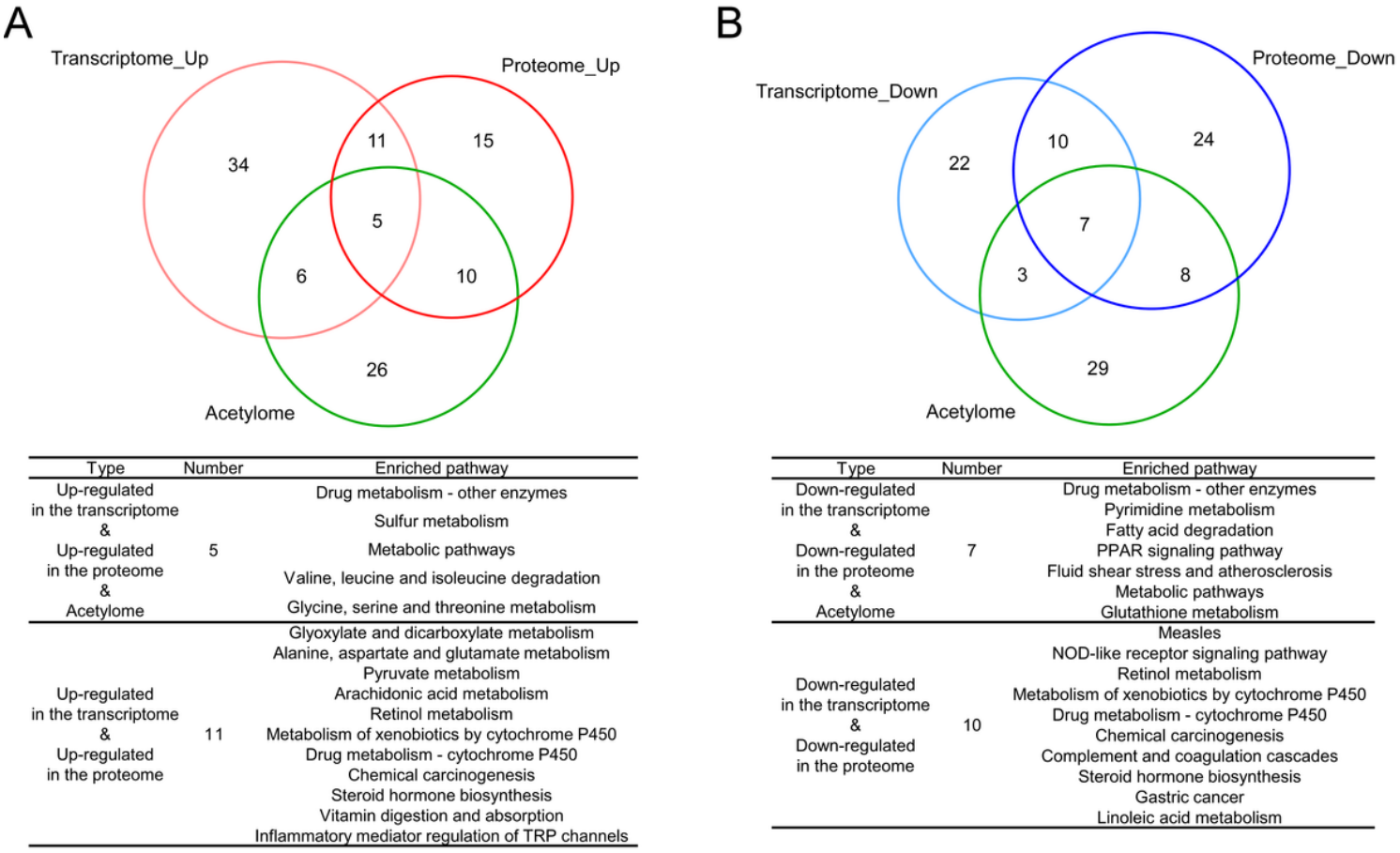

Type	Number	Enriched pathway
Up-regulated in the transcriptome & Up-regulated in the proteome & Acetylome	5	Drug metabolism - other enzymes Sulfur metabolism Metabolic pathways Valine, leucine and isoleucine degradation Glycine, serine and threonine metabolism
Up-regulated in the transcriptome & Up-regulated in the proteome	11	Glyoxylate and dicarboxylate metabolism Alanine, aspartate and glutamate metabolism Pyruvate metabolism Arachidonic acid metabolism Retinol metabolism Metabolism of xenobiotics by cytochrome P450 Drug metabolism - cytochrome P450 Chemical carcinogenesis Steroid hormone biosynthesis Vitamin digestion and absorption Inflammatory mediator regulation of TRP channels

Type	Number	Enriched pathway
Down-regulated in the transcriptome & Down-regulated in the proteome & Acetylome	7	Drug metabolism - other enzymes Pyrimidine metabolism Fatty acid degradation PPAR signaling pathway Fluid shear stress and atherosclerosis Metabolic pathways Glutathione metabolism
Down-regulated in the transcriptome & Down-regulated in the proteome	10	Measles NOD-like receptor signaling pathway Retinol metabolism Metabolism of xenobiotics by cytochrome P450 Drug metabolism - cytochrome P450 Chemical carcinogenesis Complement and coagulation cascades Steroid hormone biosynthesis Gastric cancer Linoleic acid metabolism

Figure 5

Integration of enriched pathways among the transcriptome, proteome, and acetylome. (A) Upper panel shows the Venn diagram of Transcriptome_Up, Proteome_Up, and Acetylome. Lower panel shows the specific pathway list. Transcriptome_Up: enriched pathways in up-regulated transcripts in the transcriptome. Proteome_Up: enriched pathways in up-regulated proteins in the proteome. Acetylome: enriched pathways in differentially regulated acetylated proteins. (B) Upper panel shows the Venn diagram of Transcriptome_Down, Proteome_Down, and Acetylome. Lower panel shows the specific pathway list. Transcriptome_Down: enriched pathways in down-regulated transcripts in the transcriptome. Proteome_Down: enriched pathways in down-regulated proteins in the proteome. Acetylome: enriched pathways in differentially regulated acetylated proteins. A pathway with an adjusted p-value < 0.05 (calculated by KOBAS) is considered an enriched pathway.

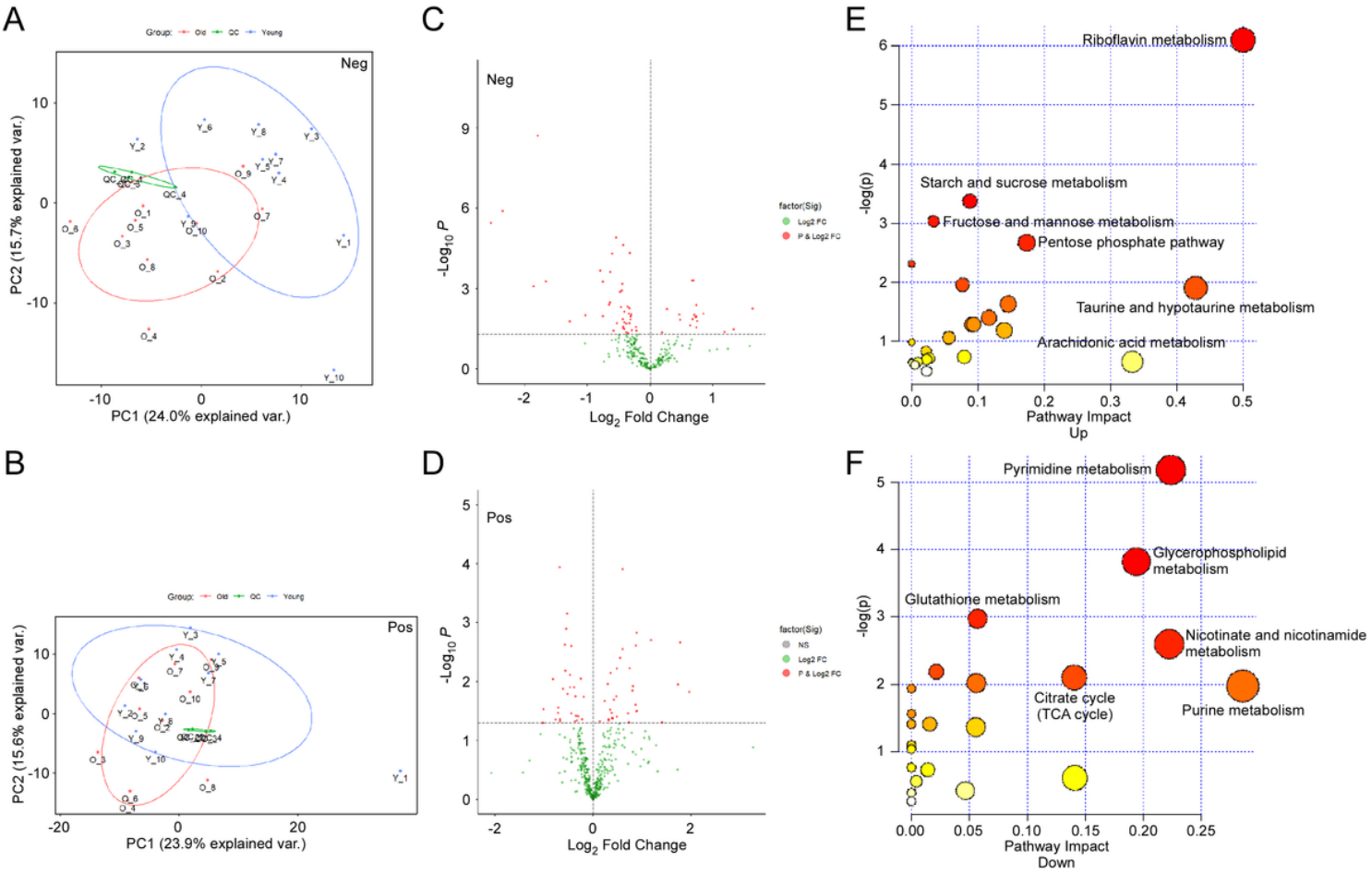

Figure 6

Hepatic metabolome of young and old mice. (A) PCA of metabolites identified in negative-ion mode. (B) PCA of metabolites identified in positive-ion mode. (C) Volcano plot of metabolites identified in negative-ion mode. (D) Volcano plot of metabolites identified in positive-ion mode. (E) Pathway analysis of the 43 up-regulated metabolites. (F) Pathway analysis of the 63 down-regulated metabolites.

Supplementary Files

This is a list of supplementary files associated with this preprint. Click to download.

- 2Supplementarymaterial.docx
- S1supplementAginglivermultiomicstrans.tif
- S2supplementAginglivermultiomicsTQ.tif
- S3supplementAginglivermultiomicsTPAc.tif
- S4supplementAginglivermultiomicsTPAc.tif
- S5supplementAginglivermultiomicsmetabo.tif
- TableS1Qualitycontrolmetricsfortranscriptome.xlsx

- TableS2TopenrichedKEGGpathwaysandtranscripts.xlsx
- TableS3TopenrichedKEGGpathwaysandproteins.xlsx
- TableS4Alterationofhistones.xlsx
- TableS5TopenrichedKEGGpathwaysandacetylatedproteins.xlsx
- TableS6Differentiallyregulatedmetabolites.xlsx